# Matching of curvilinear structures : application to the identification of cortical sulci on 3D Magnetic Resonance Brain Image

Samuel Legoupil, Houssam Fawal, Michel Desvignes, Marinette Revenu, Daniel Bloyet, Pascal Allain, Jean-Marcel Travère

# Matching of Curvilinear Structures : Application to the Identification of Cortical Sulci on 3D magnetic resonance brain image

S Legoupil, H Fawal, M Desvignes, M Revenu [1,4], D Bloyet [2,4], P Allain, JM Travere [3,4]

[1] : LAIAC-ISMRA 6 bd maréchal Juin. 14050 Caen.
[2] : LEI-ISMRA 6 bd maréchal Juin. 14050 Caen.
[3] : CYCERON/CEA. bd Becquerel. 14050 Caen.
[4] : POLE IMAGE. ISMRA 6 bd maréchal Juin. 14050 Caen.
Email : Michel.Desvignes@L2I.ISMRA.FR

## 1. INTRODUCTION

Positron Emission Tomography (PET) is a non-invasive imaging technique that provides *quantitative* maps of biochemical, biophysical and physiological parameters of the in-vivo human brain [1,2]. PET images offer imprecise anatomical information because of the poor spatial resolution, poor statistics and because the tracer does not reflect the anatomy. Accurate and reproducible analysis of PET images requires other information coming from anatomical databases or from Magnetic Resonance Image (MRI) of the same patient [3].

Conversely, Magnetic Resonance Imaging offers accurate in-vivo localisation of anatomical landmarks [4]. It has been used to estimate individual variations and left-right asymmetries of sulci and gyri. Hence, it is of great interest to superimpose functional PET data and anatomical MRI data. There are three modern approaches to this problem :

The stereotaxic proportional grid of Talairach [5] is frequently used. It defines spatial coordinates of brain sulci and gyri, and of cytoarchitectonic fields. Despite the application of scaling factors, the accuracy of the superimposition of a standard brain atlas onto any given examination is about one to two centimetres at the cortical level, because of inter-individual variations [6].

A second approach is based on templates upon a standard brain. Global deformations are sometimes integrated in this approach [7] but it seems that all inter-individual variations cannot be taken into account.

A third approach determines cortical maps based on the topology of sulci and gyri [8,9].

Our work is based on the last method. Our objective is to automatically recognize cortical sulci of any brain MRI examination, with respect to an anatomical atlas. The deformations of the sulci can be computed. In this paper, we deal with the identification of the lateral sulcus (Sylvian fissure) on 3D MR Images.

This work is partially supported by Sun Microsystem.

Previously [10], we proposed a heuristic method based on spatial location to recognize the lateral sulcus. Here, a new approach is presented, based on continuous relaxation, to identify cortical human sulci. Initial data are first described. Elastic and inexact matching are summarized. Then, we introduce our method. Finally, we present results on the lateral sulcus and give perspectives of this work.

## 2. Initial Data and Preprocessing

Brain MR Images are obtained from five young sane volunteers with a General Electric Sigma Advantage machine. No information about sex and age is available. MR Images are composed of 120 sections of 256x256 isotropic voxels ($1.3x1.3x1.3mm^3$). An automatic procedure [11] puts this set in the Talairach's coordinate system, then isolates the brain from other parts (skull, eyes orbits, skin). A multi level thresholding operation splits the set into cerebro-spinal fluid (CSF), white matter and grey matter.

A sulcus is a cerebral structure, filled with Cerebro-Spinal Fluid (CSF), at the location where the cortex enters the brain. Thus, CSF on our MR images of the brain corresponds to cortical sulci.

By application of a 3D skeletonization and skew curve thinning algorithms [12], limits of any sulcus can be drawn at the cortical level (*figure 1*).

Each sulcus is described by a graph of segments. A segment corresponds to the set of voxels lying between two intercepts. Since the Talairach's atlas gives only a rough approximation of the average landmarks, we have defined a window in which the lateral sulcus is always present. We have a limited number of segments which can belong to the lateral sulcus, in order to improve computation times. Because this sulcus is approximately situated in a plane, we use a 2D lateral projection of the image.

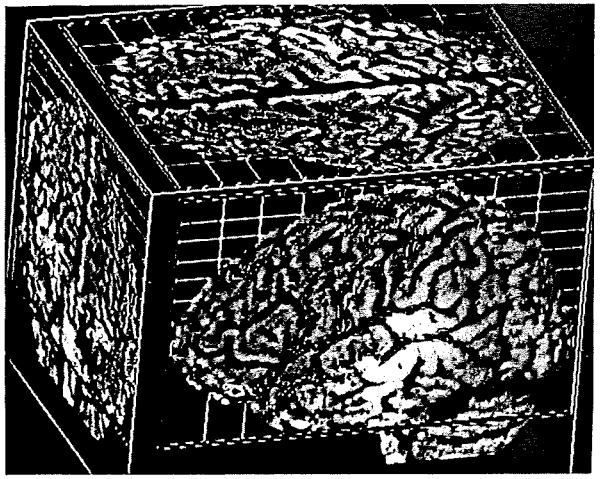

Figure 1. Initial image and skeleton

Our problem is now to find identical patterns on the Atlas and on the MR image, i.e. to find a matching between two graphs of segments. The large variety of numbers, patterns and positions of the real sulci requires elastic matching, which allows deformations. To match graphs of segments, several operations are possible :

*Deletion* or *insertion* of a segment in a graph, which corresponds to inexact matching;

*Modification* (length, orientation) of a segment in a graph, which corresponds to elastic matching.

We have combined these two operations : we first use inexact matching to determine elements shared by the two graphs. Then, deformations are computed using elastic matching.

## 3. Methods

### 3.1. Inexact matching

Three kinds of methods try to bring out the largest structures of two graphs :

*Metric methods* [13] quantize the correspondence between two graphs with similarity and correlation measures. They may be explained with the physical analogy of "templates and springs". These methods minimize a metric which depends upon three measures :

- similarity between the matched input elements' relations and the reference relations between templates;
- similarity between input data and templates;
- cost of missing elements.

*Tree search* [14] and backtracking build and explore the solution space. Although numerous variants and heuristics improve computation times, these algorithms are still time consuming. Polygamy is not allowed, i.e. one vertex of a graph cannot match two vertices on the other graph.

*Maximal cliques search* [15] is an NP-hard problem which has the same disadvantages as tree search.

*Constraint propagation* is a stochastic approach, and *relaxation* techniques [16], applied to graph matching, will be explained later.

### 3.2. Elastic matching

The intuitive idea of elastic matching is very simple : a transformation is iteratively applied to warp a graph toward another one. Formulation in terms of optimization is done by means of a cost measure. The number of iterations can be controlled by a similarity measure. Local and elastic deformations are compensated by these methods. They differ about optimization methods and deformation models.

Gee [17] use BROIT's algorithm, based on Navier's equations which describe elastic deformations of a solid. A multi-resolution stage proceeds step-by-step in a coarse to fine deformation process, increasing local similarity and global consistency. Two matching structures are used : the outer edge of the brain and the brain ventricles. The topology of these structures must be identical.

Elastic nets [18] and snakes [19] minimize a function based on geometric (angle, length, curvature, ...) and photometric (intensity) criteria. Topologically identical patterns can be processed by these methods.

Using rigid deformations, fast registration and recognition of curves and surfaces have been implemented by means of B-Splines [20].

BURR's algorithm [21] proceeds by Gaussian smoothed deformations and multi-resolution stage. This algorithm has been used on dot patterns, grey-scale 2D images and

edges in 2D medical images. It computes deformations of any point and new constraints can be easily added.

## 4. PROPOSED SYSTEM

Elastic matching methods have potential applications for graphs matching if the graphs share the same topology [22]. As a first step, segments common to the atlas and to the examined brain are retained by a bi-relaxation labeling process. As a second step, elastic matching is applied to the simplified sulcus.

The relaxation method [16] is used as a labeling process between a set of objects - sulcus to identify - and a set of labels - sulcus of an atlas. It is a parallel iterative method which optimizes the constraints to be satisfied.

### 4.1. Relaxation

Let $g$ denote a set of $n$ objects and $G$ denote a set of $N$ labels. $i$ and $I$ refer respectively to an object of $g$ and a label of $G$. $D_{ij}$ is the set of all pairs $(I;J)$ such that label $I$ at object $i$ is compatible with label $J$ at object $j$. Label pairs which are not in $D_{ij}$ represent pairs of incompatible labels at the corresponding objects $i$ and $j$.

The continuous relaxation labeling process is a stochastic approach for the identification of objects by measuring the compatibilities along arcs which define the graphs. A constraint function $R_{ij}(I;J)$ takes on real values from 0 to 1. The magnitude of $R_{ij}(I;J)$ is proportional to the strength of the constraint between pairs (unknown $i$, label $I$) and (unknown $j$, label $J$). The constraints $R_{ij}(I;J)$ when objects (or labels) are not neighbors, or for unmatching couples are null. Finally, $p_i(I)$ denotes an estimation of the likelihood that object $i$ matches label $I$ according to :

$$0 \le p_i(J) \le 1 \quad and \quad \sum_{I=1}^{N} p_i(I) = 1$$

A consistent labeling is a mapping in which all the constraints are satisfied. The prototype algorithm is a parallel iterative procedure that increasingly satisfies the constraints. At each loop, the labeling is turned into a more consistent one, by maximazing the gain A(p) defined by :

$$A(\bar{p}) = \sum_{i=1}^{n} \sum_{I} \sum_{j=1}^{n} \sum_{J} p_i(I) \times p_j(J) \times R_{ij}(I,J) \qquad with \quad I,J \in D_{ij}.$$

The gain A(p) is iteratively maximized by a gradient based optimization. Hummel and al. [15] make clear that a good approximation for the new assignment is given by :

$$p_i^k(I) = p_i^{k-1}(I)\,(1 + \sum_{j=1}^{n} \sum_{J=1}^{N} 2 \times p_j^{k-1}(J) \times R_{ij}(I,J))$$

The process is repeated until the labeling, while becoming more consistent, leads to an almost individual assignment.

### 4.2. Constraints

Relational similarities associated to constraints describe geometrical features between segments of the sulcus. We define two binary relations $\rho_1$ and $\rho_2$.

In most cases, the main characteristic of a sulcus is the continuity along segments, with short length breaks. To take this feature into account, the first relation is the smallest distance between two segments (*figure 2*), i.e. the distance of the nearest points :

$\rho_1(i;j) = dist_{min}(i;j)$

The second characteristic between two related segments is the angle between their principal axes. As the orientations of the sulcus in the Talairach's coordinate system are roughly constant, we define the second relation as the angle between the sulci's bisecting line and a determined axis :

$\rho_2(i;j) = angle(bisecting\ line\ (i;j),\ \Delta)$

The global constraint between (i;I) and (j;J) is defined by :

$$R_{ij}(I;J) = \exp\left\langle -\frac{|\rho_1(i;j) - \rho_1(I;J)|}{\sigma_1} - \frac{|\rho_2(i;j) - \rho_2(I;J)|}{\sigma_2} \right\rangle$$

The parameters $\sigma_1$ and $\sigma_2$ determine the relative influence of each relation. A maximum value of $R_{ij}(I;J)$ is obtained if the relations are equal for labels and objects. Large differences between relations yield a null value of $R_{ij}(I;J)$.

### 4.3. Bi-relaxation

A relaxation labeling process defines a homomorphism from the set of objects to a subset of labels. In practice, the relaxation process identifies one sulcus in the unknown image with respect to the atlas. Two problems must be taken into account :

- The unknown label is attributed if one segment does not exist on the atlas.
- Several segments have the same label on the atlas (many-to-one relation).

Disparities are due to inter-individual variabilities, data capture and image processing. Identical topologies are needed to compute local deformations.

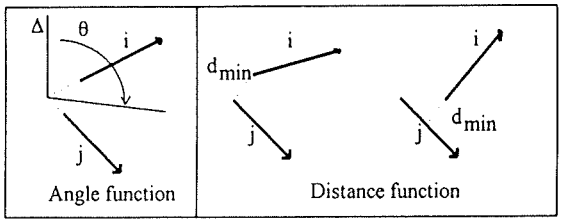


Figure 2. Relational similarities

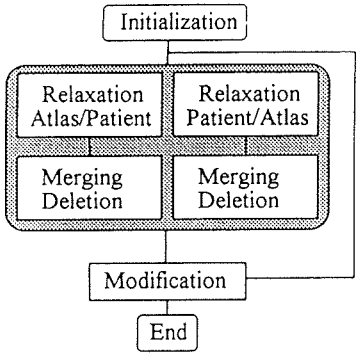


Figure 3. The bi-relaxation labeling process

In this way, we introduce two operators. A segment without relation is deleted while segments with many-to-one relations are merged.

Then, the one-to-one mapping is obtained by considering two relaxation processes, each followed by merge and remove operators. The functional diagram is shown *figure 3*. The first relaxation process, from atlas to patient, identifies segments of a patient's image which have to be removed or merged. The second one carries out the same operation onto the atlas. The process ends when no modification occurs in the two graphs. The final result is the set of segments with identical topology on the atlas and on the patient's examination.

### 4.4. Initialization

Initial values of coefficients $p_i(I)$ are usually computed from a distance based on label intrinsic features, which are *a priori* estimations.

In our problem, there are no intrisic features. The length of a sulcus depends on the real configuration of the brain and on errors in the segmentation process. The absolute position in the Talairach's system gives some information about the segment label. Depth of a sulcus is not a sufficient discriminant feature. In order to validate the proposed system on spatial relations, initial values are equally distributed.

In practice, large different numbers and lengths of segments in the two graphs decrease the efficiency of *merging* and *deletion* operators. In this case, the longest segments of the smallest graph are halved.

### 4.5. Merging and deletion

Ideally, labeling between the set of labels and the set of objects is a one-to-one mapping, i.e. :

$$\exists\ (i,I_0)\ /\ p_i(I_0) = 1 \text{ and } \forall I \neq I_0\ ,\ p_i(I) = 0,$$

but in the case of different topological configurations, although visually identical, and with the similarity relation, several segments of a graph may map a unique segment to the second one. These segments may be merged under certain conditions (*figure 4*). In the same way, segments with no matching may be removed.

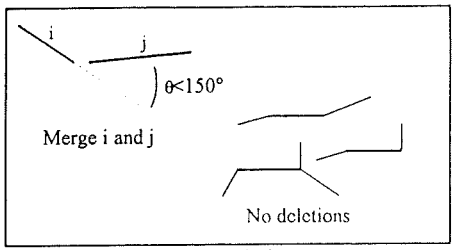


Figure 4. Merging and deletion

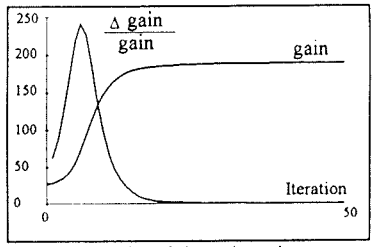


Figure 5. Gain of the relaxation

The segments are considered as neighbors if their minimum distance is less than a threshold. This threshold is equal to 10% of the average length of the segments.

*Merging* : two segments are merged if the three following conditions are satisfied :

- they are neighboring ;
- the angle between the two segments is less than 150 degrees ;
- the two segments have the same mapping in the other graph.

*Deletion* : one segment is deleted if it has no mapping in the other graph and if it cannot connect two parts of the sulcus, i.e. :

- it has exactly 2 neighboring segments and the angle between at least one of these two neighbors and the examined segment is less than 150 degrees ;
- it has more than 2 neighboring segments.

### 4.6. Control

The gain of the relaxation process is defined as the last value of A(p). Variations are shown *figure 5*. The function Δgain/gain determines the end of the process. A threshold value has been fixed to $10^{-5}$ (*figure 5*).

Let *ng* and *NG* (resp. *gain* and *GAIN*) denote the final segments numbers (resp. the final values of A(p)) in each relaxation process. The function $\phi(\sigma_1,\sigma_2)$ is defined by :

$$\phi(s_1,s_1) = \frac{gain}{ng} - \frac{GAIN}{nG}$$

$\phi(\sigma_1,\sigma_2)$ is the gain's difference scaled to the unit of segment. $\phi(\sigma_1,\sigma_2)$ estimates the fitness of the matching if less than 50% of segments have not been cancelled by the deletion operator. Optimal values of $\sigma_1$ and $\sigma_2$ are automatically estimated using this function.

### 4.7. Deformations

The computation of deformations between the MR Image and the atlas is based on Burr's algorithm [21].

As a first step, correspondences between voxels in contours in the two images are used to stretch one image (patient's image) toward its goal (atlas). Gaussian smoothed deformation is used to match contours. As a second step, the resulting stretched image is used to warp it further toward its goal, using Gaussian smoothed deformations. The process is iterated with decreasing stiffness. As iterations continue, the resulting image better approximates the goal image.

Let $T(x_i,y_i,z_i)$ denote the displacement vector of the matched contours obtained after the first step. The distortion vector at a point M(x,y,z) is given by :

$$V(x,y,z) = \frac{\sum_{i=1}^{N_s} F_i(x,y,z) \times (T(x_i,y_i,z_i) - \frac{1}{N_s} \cdot \sum_{i=1}^{N_s} T(x_i,y_i,z_i))}{\sum_{i=1}^{N_s} F_i(x,y,z)}$$

*with*

$$F_i(x,y,z) = \exp\left(\frac{-(x-x_i)^2 - (y-y_i)^2 - (z-z_i)^2}{b^2}\right)$$

The parameter $\beta$ is an elasticity constant. A large elasticity constant results in more significant weight distant points and the image becomes more elastic. For small elasticity constant, the image becomes more rigid and deformations are interpolated locally. In practice, the process starts with a large value of $\beta$. In subsequent iterations the value of $\beta$ is gradually decreased.

This method has been used in three dimensions and the results are satisfactory when the graphs to be matched have the same topology. The correspondence between the 2D inexact matching of the lateral sulcus and the 3D elastic deformation is actually established manually.

## 5. Experiments and Results

### 5.1. Results

To validate our approach, we have simulated an anatomical atlas by an MR Image. Our experiments are based on 55 pairs of lateral sulci. This sulcus, which is always visible on an MR Image, shows large asymmetries between the left and right hemisphere of the same patient. It shows also a different number of parts and a lot of variation in the positions of these parts, from patient to patient. The identification of this sulcus represents a complete coverage of the main recognition problems of other sulci. Moreover, the lateral sulcus is simple to detect and to be manually checked.

*Figure 6* illustrates the difficulties. The final result is two sulci of identical topologies. On the set of 55 pairs, 48 have given exact matching while 7 have failed. The failures are due to two images in which the position of the lateral sulcus with respect to Talairach's atlas shows a large difference. It seems that the accuracy of orientation must be better than 30 degrees.

### 5.2. Parameters

The function $\phi$ estimates the smoothness of a matching, in order to define experimental values of the parameters $\sigma_1$ and $\sigma_2$. Qualitatively, we have defined three levels of smoothness :

- A null value of $\phi$ leads to an exact matching (*figure 7*);
- An intermediate value of $\phi$ leads to a correct matching;
- A large value gives an incorrect matching.

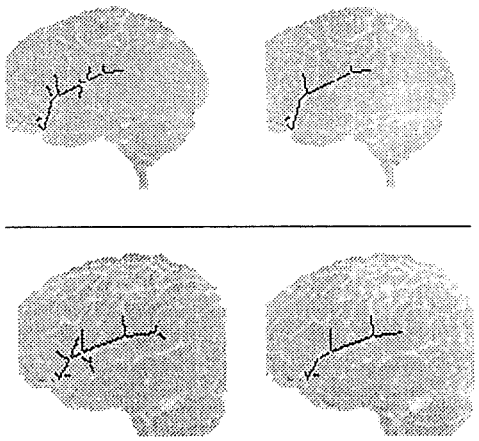

Figure 6. Example : on the left side, the simulated atlas and patient image skeleton. On the right side, common parts of the lateral sulcus on the initial image

| | Example 1 | Exact | Example 2 | Correct | Example 3 | False |
|---|---|---|---|---|---|---|
| Step | - 1 - | - 3 - | - 1 - | - 2 - | - 1 - | - 5 - |
| gain | 193.3 | 114.4 | 97.03 | 78.6 | 203.2 | 120.3 |
| GAIN | 196.9 | 111.4 | 98.9 | 83.9 | 110.8 | 61.6 |
| ng | 21 | 13 | 20 | 17 | 22 | 16 |
| nG | 20 | 13 | 22 | 18 | 15 | 10 |
| $\phi$ | -0.64 | *0.0* | 0.34 | *-0.04* | 1.8 | *1.35* |

Figure 7. Function $\phi(\sigma_1,\sigma_2)$ in 3 typical cases

Function $\phi$ reaches definitely a minimum for a smooth matching. Conversely, this minimum specifies the parameters which provide an exact matching. Each of 55 examples has been tested for different values of $\sigma_1$ and $\sigma_2$. These tests have established two points :

- A satisfactory matching corresponds to a minimum of $\phi$
- On the set of 55 pairs, a standard set of parameters $\sigma_{1s}$ and $\sigma_{2s}$ provides 48 correct matchings.

## 6. Conclusion

The initial goal of this work was the identification of segments describing the sulcus on MR Images. The deformation, computed by an elastic matching, has led to the necessity of identical topology and the resort to the system proposed.

This approach, based on relaxation, models relational geometric features between elements of a sulcus and between sulci, in order to build common sets of segments. Results are

satisfactory to recognize lateral sulci on 2D MR Images. The parameters $\sigma_1$ and $\sigma_2$ can be obtained from a set of tests.

We presently work on the generalisation of 3D geometrical relations and the extension to other sulci of brain MRI examinations by integrating relations between sulci and other structures like ventricles.

## REFERENCES


1. Fox PT, Perlmutter JS, Raichle ME. A stereotactic method of anatomical localization for positron emission tomography. *J. Comp. Assist. Tomogr.*. 1985; 9 :141-153.
2. Neelin P, Crossman J, Hawkes DJ, Ma Y, Evans AC. Validation of an MRI/PET landmark registration method using 3D simultated PET images and point simulations. *3D Advanced image processing in medecine. 14th IEEE EMBS* 1992. pp 73-78.
3. Evans AC, Marrett S, Torrescorzo J, Ku S, Collins S. MRI/PET correlation in 3D using a volume of interest (VOI) atlas. *J. of cerebral flow and metabolism*. 11, pp A69-A78, 1991.
4. Rademacher J, Galaburda AM, Kenedy DN, Filipek PA, Caviness VS. Human Cerebral cortex : localization, parcellation and morphometry with magnetic resonance. Imaging, *J. of cognitive neuroscience*, 4, 4, pp352-374. 1992.
5. Talairach J, Tournoux P. Co-planar stereotaxic atlas of the human brain. New York Thieme. 1988.
6. Allain P, Travere JM, Baron JC, Bloyet D. 3D superimposition and fitting of a stereotaxic atlas onto 3D MRI and PET brain images. *4th inter. Symposium on Biomedical engineering*,. pp Peniscola, Spain, 1991.
7. Greitz T, Bohm C, Holte S, Eriksson L. A computerized brain atlas : construction, anatomical content and some applications. *J. of computer assisted tomography*, 15, pp 26-38. 1991.
8. Rademacher J, Caviness VS, Steinmetz H, Galaburda AM. Topographical variation of the Human Primary Corices : implications for neuroimaging, brain mapping and neurobiology. Cerebral Cortex, 3, pp313-329. 1993
9. Jouandet ML, Tramo MJ, Herron DM, Hermann A, Loftus WC, Bazell J,Gazzaniga MS. Brainprints : computer generated two dimensional maps of the human cerebral cortex in vivo. *J. of Cognitive Neuroscience*. 1,1, pp88-117. 1989.
10. Desvignes M, Fawal H, Revenu M, Bloyet D, Allain P, Travere JM, Baron JC. Reconnaissance du sillon latéral sur image RMN 3D. RFIA. Paris 1994.
11. Allain P, Travere JM, Baron JC, Bloyet D, Desvignes M. Entirely automatic 3D MRI brain analysis as a step in multi modal processing. *14th IEEE EMBS*.1992. pp 947-951.
12. Desvignes M, Fawal H, Revenu M, Bloyet D, Allain P, Travere JM, Baron JC. Calcul de la profondeur en un point des sillons du cortex. *GRETSI*. Juan les Pins. 1993
13. Ballard DH, Braun CM. *Computer Vision*. Prentice Hall 1982.
14. Vosselman G. Relational Matching. *Lecture Notes in computer science*, 628. 1992
15. Miclet L. Méthodes structurelles pour la reconnaissance des formes. *Eyrolles*. 1984
16. Hummel RA., Zucker SW. On the Foundations of Relaxation Labeling Processes - *IEEE.PAMI*, vol 5, No.1, 1983.
17. Gee JC, Reivich M, Bajcsy R. Elastically deforming 3D atlas to match anatomical brain images. *J. Comp. Assit. Tomogr.*. 1993; 17 :225-236.
18. Bertille JM. Le réseau élastique appliqué à la reconnaissance des chiffres manuscrits. *RFIA*. Paris 1994.
19. Kass M., Terzopoulos D., Wintkin A..Snakes : active contours models. *3rd Int. Conf. on Comp. Vision*. pp 259-268. 1987.
20. Gueziec A, Ayache N. Large deformable splines, Crest lines and matching. *4th Int. Conf. on Computer Vision*. Berlin, june 1993.
21. Burr DJ. A dynamic model for image registration. *Comp. Graph. and Ima. Processing*, 15:102-112. 1981.
22. Desvignes M., Legoupil S. Mise en correspondance d'images RMN de cerveaux. *Rapport interne LAIAC*. Avril 1994.